Full bandgap defect state characterization of β-Ga₂O₃ grown by metal organic chemical vapor deposition

Hemant Ghadi, Joe F. McGlone, Christine M. Jackson, Esmat Farzana, Zixuan Feng, A F M Anhar Uddin Bhuiyan, Hongping Zhao^{1,2}, Aaron R. Arehart and Steven A. Ringel^{a)}

A detailed investigation into electrically-active defects within high-mobility, MOCVD-grown β-Ga₂O₃ epitaxial layers are reported in this article. A net doping concentration of 1.2×10¹⁷ cm⁻³ and a high electron mobility of 152 cm²/Vs at 300 K were measured by using C-V profiling and Hall-effect measurements, respectively. The trap state which dominates the entire defect spectrum was a relatively shallow state at E_C-0.12 eV and the measured concentration was on par with values reported from transport studies. Deep level transient spectroscopy revealed a unique trap at E_C-0.4 eV that is distinct from all other reported traps in β-Ga₂O₃. Moreover, deep level optical spectroscopy at 300 K detected three defect states at Ec-1.2, Ec-2.0, and Ec-4.4 eV, with at least one order of magnitude lower concentration than previous reports. The key finding of this work is to highlight significantly lower concentrations of measured traps in MOCVD grown β-Ga₂O₃ compared to any other growth methods reported thus far, as well as the observation of a unique trap at Ec-0.4 eV. A significant reduction in overall trap concentration using the MOCVD growth technique when compared to prior work on MBE-grown and bulk substrates suggests that ionized impurity scattering plays a major role in limiting mobility. Possible connections between the remarkably low overall trap concentration, and the observed high mobility is presented, with the goal towards guiding the synthesis of high performance MOCVD-grown devices in the future.

¹Department of Electrical and Computer Engineering, the Ohio State University, Columbus, Ohio 43210, USA

²Department of Materials Science and Engineering, The Ohio State University, Columbus, Ohio, 43210, USA

Beta-phase gallium oxide (β-Ga₂O₃) is a promising candidate material for applications in high-power RF electronics due to its wide bandgap of ~ 4.5 -4.8 eV ¹⁻³, the ability to achieve (Al_xGa_{1-x})₂O₃/Ga₂O₃ heterojunctions ⁴, its ease of n-type doping ^{5,6}, and the availability of large area, melt-grown β-Ga₂O₃ substrates. Theoretical predictions suggest the possibility of achieving very large breakdown fields of ~ 8 MV/cm ^{7,8} and figures of merit that can exceed those of GaN and SiC. ^{8,9} The availability of native β-Ga₂O₃ substrates enables homoepitaxial growth of β-Ga₂O₃ device layers, which implies high device reliability in future applications since high concentrations of dislocations in epitaxial devices are not anticipated. As a result of these properties there has been a surge in research efforts focused on β-Ga₂O₃ over the past several years. With regard to epitaxial structures, β-Ga₂O₃ grown by molecular beam epitaxy (MBE) is being widely explored, with efforts on growth optimization, doping, heterostructure development, device characterization and defect investigations all ongoing. 10-12 MBE-based devices have yielded promising results, including δ-doped MESFETs with cut-off frequencies of 27 GHz ¹³, FINFET devices with breakdown voltages exceeding 1.6 kV ¹⁴, high fidelity field plated Schottky barrier diodes and rectifiers ^{15–17}, high 2DEG charge densities in (Al_xGa_{1-x})₂O₃/Ga₂O₃ MODFETS ^{12,18} and superior power switching figure of merits in enhancement mode β-Ga₂O₃ transistors. ¹⁹ While MBE-grown gallium oxide materials and devices are continuing to advance in performance at an accelerated pace for several years, β-Ga₂O₃ epitaxial layers grown by metalorganic chemical vapor deposition (MOCVD) is at a comparatively earlier stage of development. ^{20,21} In spite of this, very promising early reports have already established that MOCVD-grown β-Ga₂O₃ can produce transport characteristics at a materials level that are at least on par, if not exceeding, state-of-the-art MBEgrown bulk electron mobility values ^{22,23} with room temperature electron mobilities of up to 184 cm²/V-sec reported for lightly Si-doped epitaxial β-Ga₂O₃ layers. ²⁰ This impressive result implies a low concentration of defects for these MOCVD films. However, unlike the case for β-Ga₂O₃ grown by both MBE and bulk-growth methods where defect states in the bandgap have now been extensively reported ¹⁰, only sparse information currently exists regarding deep levels in MOCVDgrown β-Ga₂O₃, and those reports only cover a limited portion of the bandgap. ²⁴ Determining the entire deep level distribution in the bandgap is necessary to identify key defects that cause issues impacting device performance, such as carrier compensation, recombination-generation, trapping, scattering, and so forth. Comparison of the deep level defect distribution with reports for β-Ga₂O₃ grown by other methods ^{10,25}, and also comparing to theoretically-calculated energy levels ^{5,26,27}. can give clues regarding their physical sources, and as such, can provide guidelines for continued materials optimization. This work reports the energy and concentration profiles of bandgap states within MOVCD-grown β-Ga₂O₃ using a combination of Deep Level Optical Spectroscopy (DLOS), Deep Level Transient (thermal) Spectroscopy (DLTS), and Admittance Spectroscopy (AS).

Samples for this study were grown in an Agnitron Agilis R&D low pressure MOCVD system using TEGa (triethylgallium) and O_2 precursors. Test layers were grown to a target thickness of 1 µm using a nominal Si target doping of 1×10^{17} cm⁻³, which was confirmed by secondary ion mass spectrometry (SIMS) measurements. Intentional Si doping was used to ensure a uniform, well-controlled and low concentration doping profile to enhance trap spectroscopy analysis. The layers were grown on commercially available (Tamura) Sn-doped (010) EFG (edge-defined film fed growth) substrates at a growth temperature of 880°C using a growth rate of 0.7 µm/hour. As noted above, MOCVD-grown UID β -Ga₂O₃ layers using these same growth conditions revealed a room temperature electron mobility of 184 cm²/V-sec (4984 cm²/V-sec at 45 K), with a n-type doping concentration of 2.5×10^{16} cm⁻³ at 300 K ²⁰. Complete details of the

MOCVD growth can be found in Feng *et.al* 20 . Once grown, the structures were processed into Ni Schottky barrier diodes for subsequent electrical and defect spectroscopy measurements using standard photolithographic processes 10,25 . Ni was deposited by electron beam evaporation to a thickness of 8 nm, thin enough to allow light penetration for DLOS studies, but also robust enough for DLTS and admittance spectroscopy measurements. The Schottky contact area was 8.41×10^{-4} cm². A mesa etch was performed using BCl₃/Ar chemistry to isolate the devices. Lastly, an ohmic stack of Ti/Al/Ni/Au was deposited on the front side after a mesa isolation etch was performed. Full device processing details have been previously published, following our standard approach for DLOS and DLTS studies of β -Ga₂O₃ Schottky diodes. 10,25

Test structures were screened to ensure high quality devices were being used via the following methods: Hall effect, current-voltage (IV), capacitance-voltage (CV), and internal photoemission (IPE). Figure 1 shows representative IV, CV, and CV-extracted net ionized doping concentrations, all of which revealed consistent and high quality devices suitable for defect spectroscopy. Diode ideality factors at 300 K ranged from 1.02-1.07 for the 10 devices fabricated on this substrate, which is consistent with a nearly ideal thermionic emission-controlled Schottky diode. IPE measurements across all 10 diodes were very consistent, revealing a Schottky barrier height of $1.4 \text{ V} \pm 0.1 \text{ V}$. The extracted net ionized doping concentration from C-V was 1.2×10^{17} cm⁻³ close to the target value noted above. A separate sample grown for Hall studies under identical growth and doping conditions revealed this layer to have an electron mobility of $152 \text{ cm}^2/\text{Vs}$ at 300 K, which follows the expected trend with carrier concentration based on the earlier UID results of Feng *et al.* 20

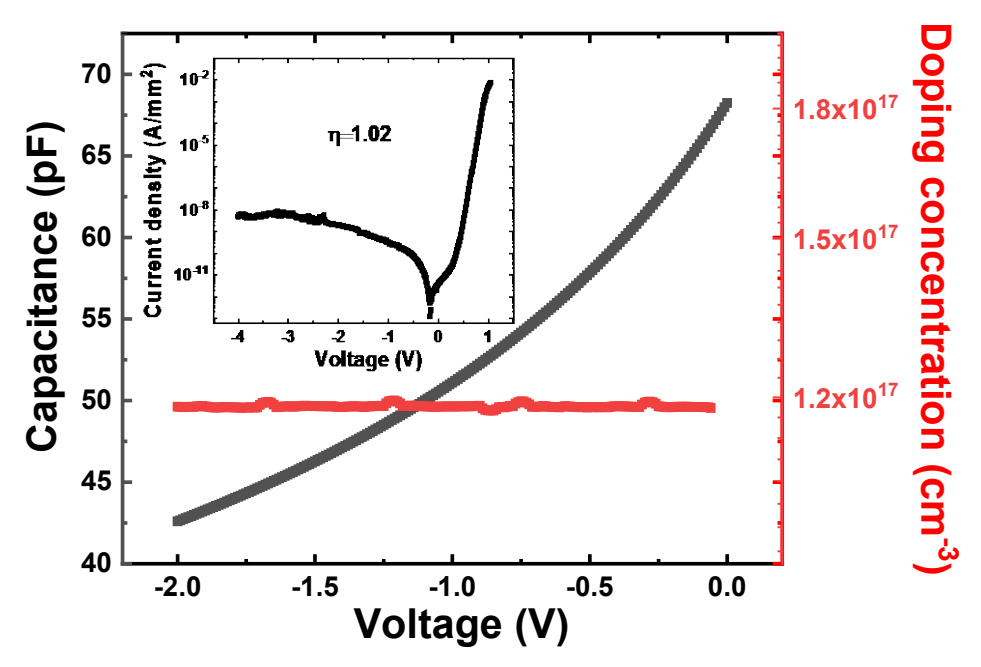


Figure 1: Room temperature CV characteristics of a typical Ni/ β -Ga₂O₃ Schottky diode and the extracted net ionized doping concentration measured at 300 K. The inset shows a typical log J vs V characteristic measured at 300 K, with an ideality factor of 1.02.

With the quality of the test devices established, defect spectroscopy could commence. Following our prior work on MBE and EFG-grown β-Ga₂O₃, both DLTS and DLOS measurements were used to probe the full range of bandgap states. Complete details of both DLTS and DLOS measurements can be found elsewhere, but are briefly outlined here. ^{28,29} DLTS measurements were performed using a fill pulse bias of 0 V with a 10 msec duration to fill trap states. To monitor the thermally stimulated carrier emission processes, a quiescent reverse bias of -2 V was used. The capacitance transients were recorded over a temperature range from 80 K to 400 K in steps of 0.1 K. The temperature-dependent capacitance transient spectra were analyzed using a conventional double boxcar method across a wide range of rate windows from 0.8 s⁻¹ to 2000 s⁻¹. With these measurements conditions, the thermally-stimulated emission based DLTS method typically can provide trap information for states with activation energies of approximately up to 1 eV. The remainder of the bandgap was probed using DLOS, wherein optical stimulation of carriers from deep levels in the bandgap is used to overcome the carrier freeze-out limitation issue for DLTS for states that exist with activation energies greater than 1 eV, all the way to the bandgap energy. In our DLOS setup, photoemission transients were measured for 300 seconds as a function of incident photon energy using a spectrally resolved, monochromatic sub-bandgap light source, at 300 K. Two different light sources, a Qth lamp (600 W) and a Xenon lamp (1000 W), were dispersed through a high resolution monochromator to provide a tunable, high resolution light source ranging in energy from 0.5 eV to 5.0 eV in 0.02 eV increments. Trap filling and quiescent biases were the same as used for the DLTS measurements except the fill pulse duration was increased to 10 sec as discussed in prior publications. ^{10,25} The steady state photocapacitance (SSPC) as a function of incident photon energy was used to extract concentrations of DLOS-detected traps, with the SSPC onset energies being indicative of the trap energies. More precise determination of the DLOS trap energy levels, and associated Frank-Condon energies were extracted by modeling of the photocapacitance transients through fitting to the Passler model of optical cross-sections. ³⁰ A more detailed description of the extraction of precise energies associated with DLOS-detected states has been published previously. ¹⁰

DLTS measurements were performed on multiple devices to ensure consistency in the results. A representative DLTS spectrum is shown in Figure 2a, revealing the presence of a single trap having an activation energy of E_C-0.4 eV. The concentration of this trap was calculated to be 3×10¹³ cm⁻³, taking into account the so-called lambda effect, which accounts and corrects for nonuniform ionization of the Ec-0.4 eV trap throughout the entire depletion region at the bias conditions used. ²⁸ The extracted capture cross-section for this trap was 1.5×10⁻¹⁴ cm², with the associated Arrhenius behavior shown in figure 2b, for which this state appears distinct from our previous DLTS studies made on both Ge-doped PAMBE 10 and unintentionally doped (UID) EFGgrown materials. ²⁵ Also shown in figure 2a is a simulated DLTS peak response calculated for an ideal, isolated, non-interacting trap state having the same energy level and capture cross section values as the measured trap. ²⁹ The excellent fit to this simple model implies that the source for this trap is likely to be a simple point defect. Interestingly, an ongoing study in our group on high energy proton radiation effects on the MOCVD material reveals the concentration of this trap is not affected by the irradiation fluence. Taken together, these results suggest that an extrinsic point defect impurity might be a possible source for this trap. Further work to explore the physical source for this trap is ongoing.

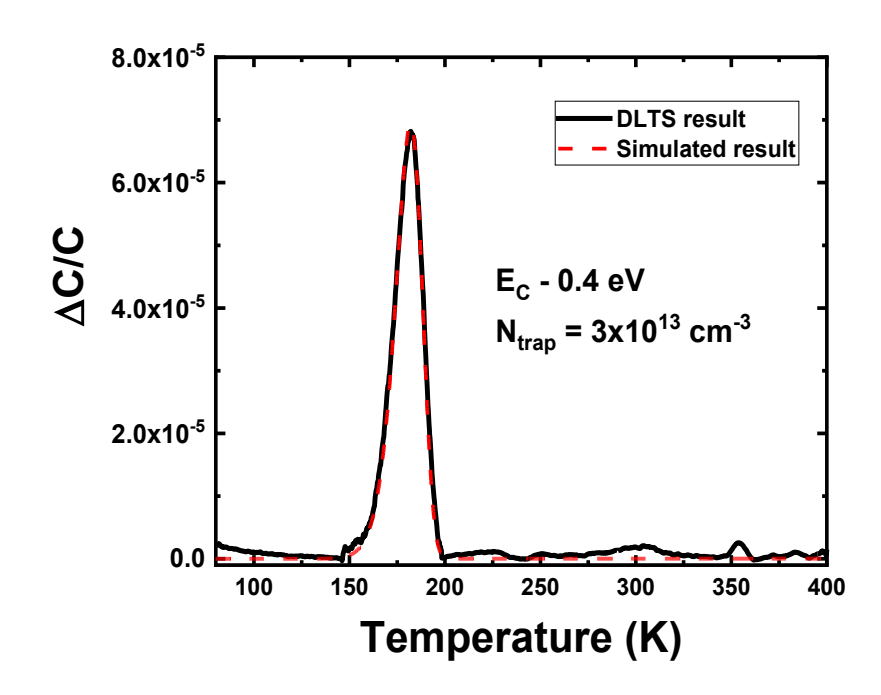


Figure 2a: DLTS spectrum exhibiting single trap emission peak at E_C -0.4 eV for a particular rate window (4 s⁻¹) compared with simulated results.

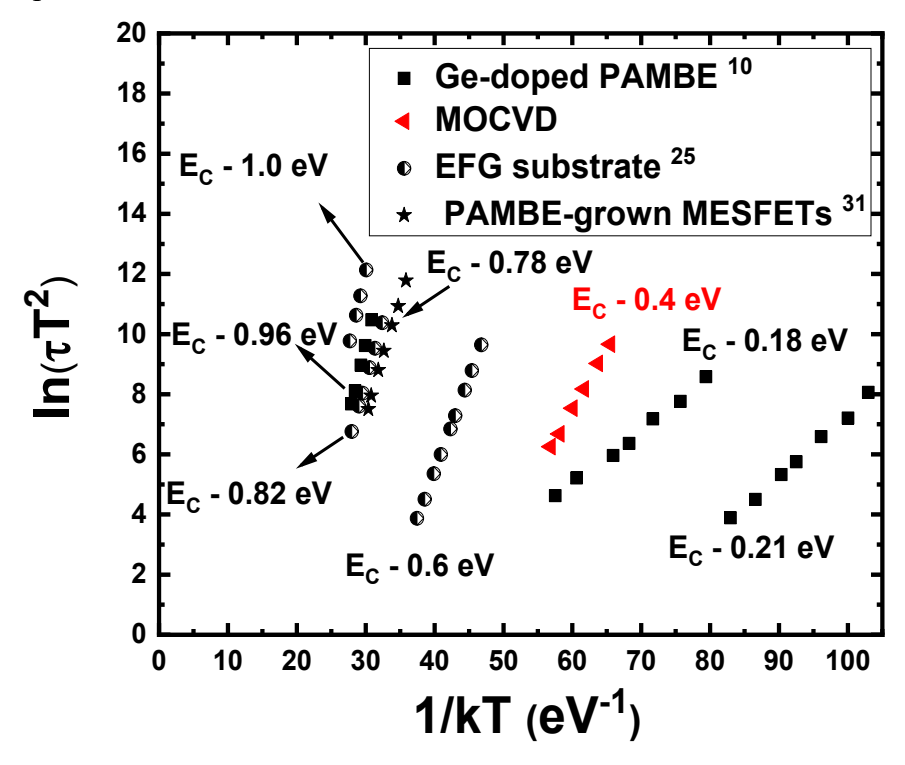


Figure 2b: Arrhenius data for this trap in MOCVD-grown β-Ga₂O₃ compared with our prior DLTS studies of β-Ga₂O₃ materials grown by PAMBE ¹⁰, EFG ²⁵ and within PAMBE-grown MESFETs. ³¹

With DLTS establishing the trap spectrum in the upper region of the bandgap, we now turn to DLOS for the remainder of the bandgap. Figure 3a shows a representative steady state photocapacitance (SSPC) spectrum with three positive photo-capacitance onsets indicated by the arrows, with the lowest energy SSPC onset magnified in the inset of figure 3a. While the SSPC onset energies indicate the incident optical energies at which the photoemission affects the photocapacitance, fitting of the optical cross section data derived from the photocapacitance transients enables more accurate determination of each trap energy level and their associated Frank-Condon energy (D_{FC}). ^{30,32} Figure 3b shows the optical cross-section data fitted using the Passler model, from which energy levels and D_{FC} values are obtained. ^{10,30,32} From this fitting the three DLOS-detected states were determined to have energy levels of E_C-1.2 eV, E_C-2.0 eV and E_C-4.4 eV, with associated D_{FC} values of 0.45 eV, 0.48 eV and 0.06 eV, respectively. These three states closely match DLOS-detected states previously reported for β-Ga₂O₃ grown by MBE ¹⁰ and EFG ²⁵, suggestive of common physical sources. There have been several efforts to explore physical sources of these states and their relative impact on material properties for MBE and EFG materials and these are briefly discussed to assist in source identification, and differentiation, for the MOCVD materials studied in this work. ^{10,25} Our prior work has shown that both E_C-1.2 eV and E_C-2.0 eV traps are sensitive to high-energy neutron irradiation, each with different defect introduction rates. 33 Moreover, it was found that these two states are the primary compensating deep levels causing carrier removal after neutron irradiation. The sensitivity to radiation fluence implies that intrinsic physical sources, such as vacancies, self-interstitials, or possible point defect complexes involving native defects are most likely responsible for these states. In fact, recent studies have shown a strong correlation between the E_C-2.0 eV state and the presence of 2V_{Ga}-Ga_i complexes based on a combination of high resolution electron microscopy studies and density functional theory (DFT) calculations. ^{34,35} That the Ec-2.0 eV trap concentration obtained from DLOS for the MOCVD β-Ga₂O₃ material here is approximately 20x less than what has been observed for MBE and EFG materials (discussed below, and shown in figure 4) implies a dependence on growth method. Such a dependence on differences between MOCVD, MBE and EFG growth conditions would not be surprising if a native defect source is linked to this state.

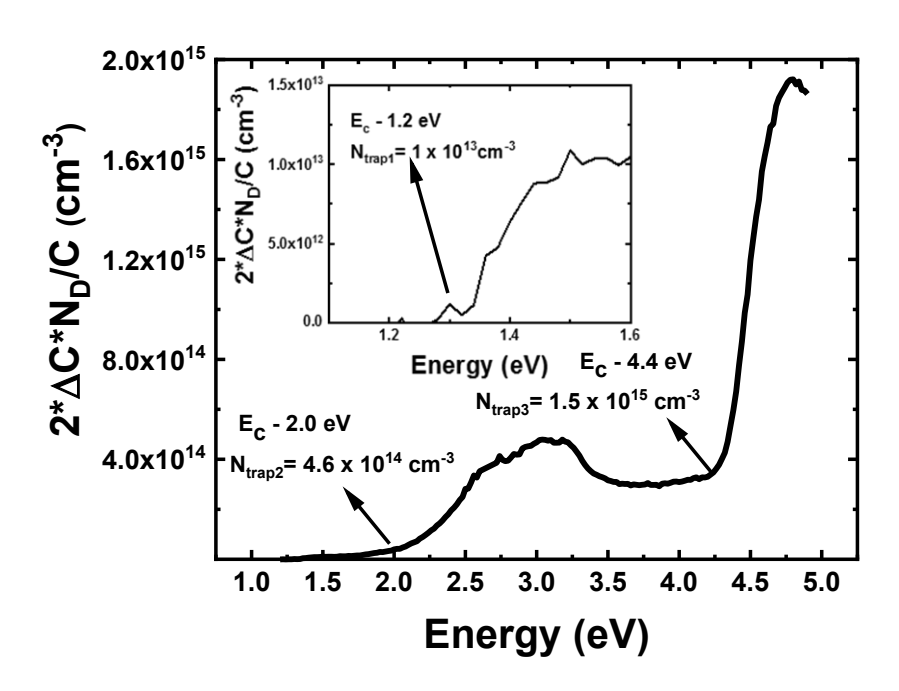


Figure 3a: Steady state photo capacitance (SSPC) spectra at 300 Kon MOCVD-grown β-Ga₂O₃. The inset shows the MOCVD SSPC measured for E_C -1.2 eV state.

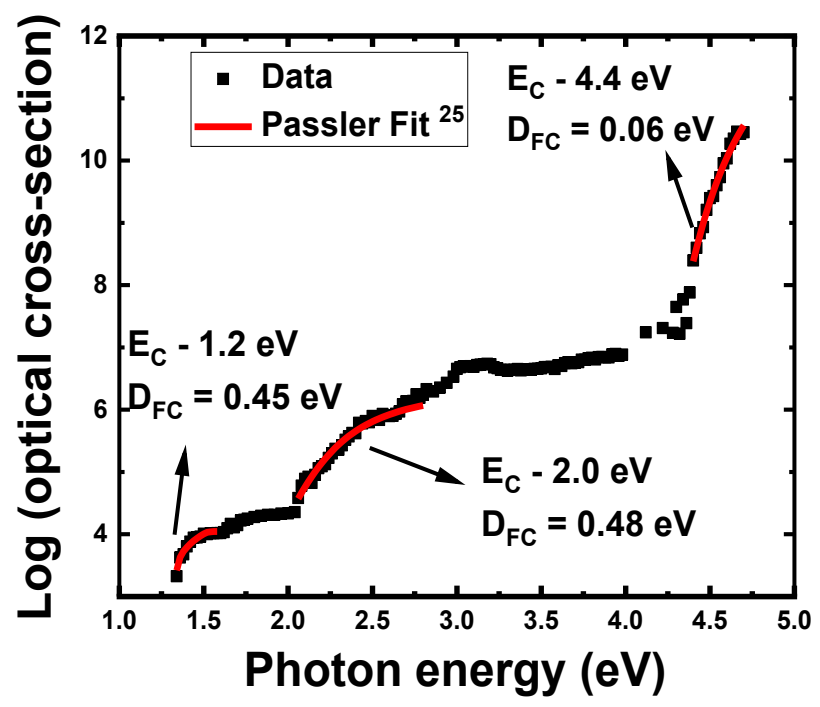


Figure 3b: DLOS optical capture cross section spectrum for MOCVD-grown β -Ga₂O₃, with the solid lines showing the fitting results using the Passler model. ³⁰

The SSPC spectrum in figure 3a also shows the presence of a negative slope starting near 3.2 eV, which is perceptible in the optical cross section data in figure 3b. This feature has been occasionally observed in earlier DLOS studies on PAMBE ¹⁰ and EFG materials. ²⁵ While the source of this feature is unclear, it is reproducible and prominent for the MOCVD material and thus merits discussion. The negative slope indicates that a significant increase in negative space charge must occur (which was confirmed by an observed a change in the sign of the photocapacitance transient data in this energy range). There are two possible explanations. First is that when the incident photon energy is greater than half the bandgap (approximately 2.4 eV for β-Ga₂O₃), competition between electron emission to the conduction band and electron capture from (i.e. hole emission to) the valence band is possible for a given state. ³⁶ Therefore, an incident flux of 2.8 eV photons can simultaneously empty the E_C-2.0 eV state to the conduction band and can capture an electron from (emit a hole to) the valence band. If the latter process becomes significant, the observed SSPC magnitude would result from a competition between the two processes, and, depending on the relative magnitudes of both emission processes, could even reduce the net SSPC magnitude, which is consistent with what is seen in figure 3a. A second possible explanation involves self-trapped holes, for which an energy level at E_V+3.1 eV has been theoretically predicted by DFT calculations. ³⁷ Hole emission to (electron capture from) the valence band to this state would also contribute a negative photocapacitance transient due to an increase in negative space charge near this photon energy, competing with the positive space charge transient due to electron emission from the E_C-2.0 eV state to the conduction band, thus explaining the observation here. At present, deciphering which process is responsible for the negatively-sloped SSPC feature requires additional investigation.

Moving now to the state at E_C -4.4 eV, we first note that this level has been observed in all DLOS studies of β-Ga₂O₃ to date, regardless of growth method, and its concentration has not appeared to vary significantly across a wide range of samples grown under different conditions, as a function of doping, or even after high energy neutron and proton irradiations. ^{10,25,33} This apparent invariance for the E_C-4.4 eV state has led to speculation that the source for this feature might be related to a fundamental property of gallium oxide itself, including the possible role of self-trapped holes, which has been very tentatively suggested previously. 38 However, such an association is inconsistent with the observation seen here on the MOCVD materials, where a very large reduction in the concentration of the E_C-4.4 eV state concentration is seen. A comparison of SSPC spectra at the same scale for β-Ga₂O₃ grown by MOCVD versus our prior work on MBE and EFG materials is provided in Figure 4. All measurements were performed under identical conditions so meaningful comparisons are established. It is very clear that all of the DLOS-detected states are greatly diminished in their concentrations for MOCVD-grown material. Since bandgap states in the range of detection for DLOS are very likely to be acceptor-like in this n-type material, such low concentrations are consistent with the low concentration of total compensating acceptors (~9x10¹⁴ cm⁻³) extracted from the transport studies published previously on the high mobility UID MOCVD material ²⁰. The large overall reduction in total trap concentration by approximately 10x for MOCVD material is significant, given the similarities observed in prior studies, and is consistent with the measured high 300 K electron mobility of 152 cm²/V-s for this lightly Si-doped sample. Furthermore, with regard to the E_C-4.4 eV state, its significant reduction in concentration here, coupled with the lack of any dependence on high-energy particle irradiation observed in earlier work, implies that an extrinsic source may be responsible. While more work is needed to discern the source of the E_C-4.4 eV state, especially given its relative dominance in the deep state concentration profiles reported to date, this tentative association with an extrinsic defect source is the first significant correlation of this state with growth conditions.

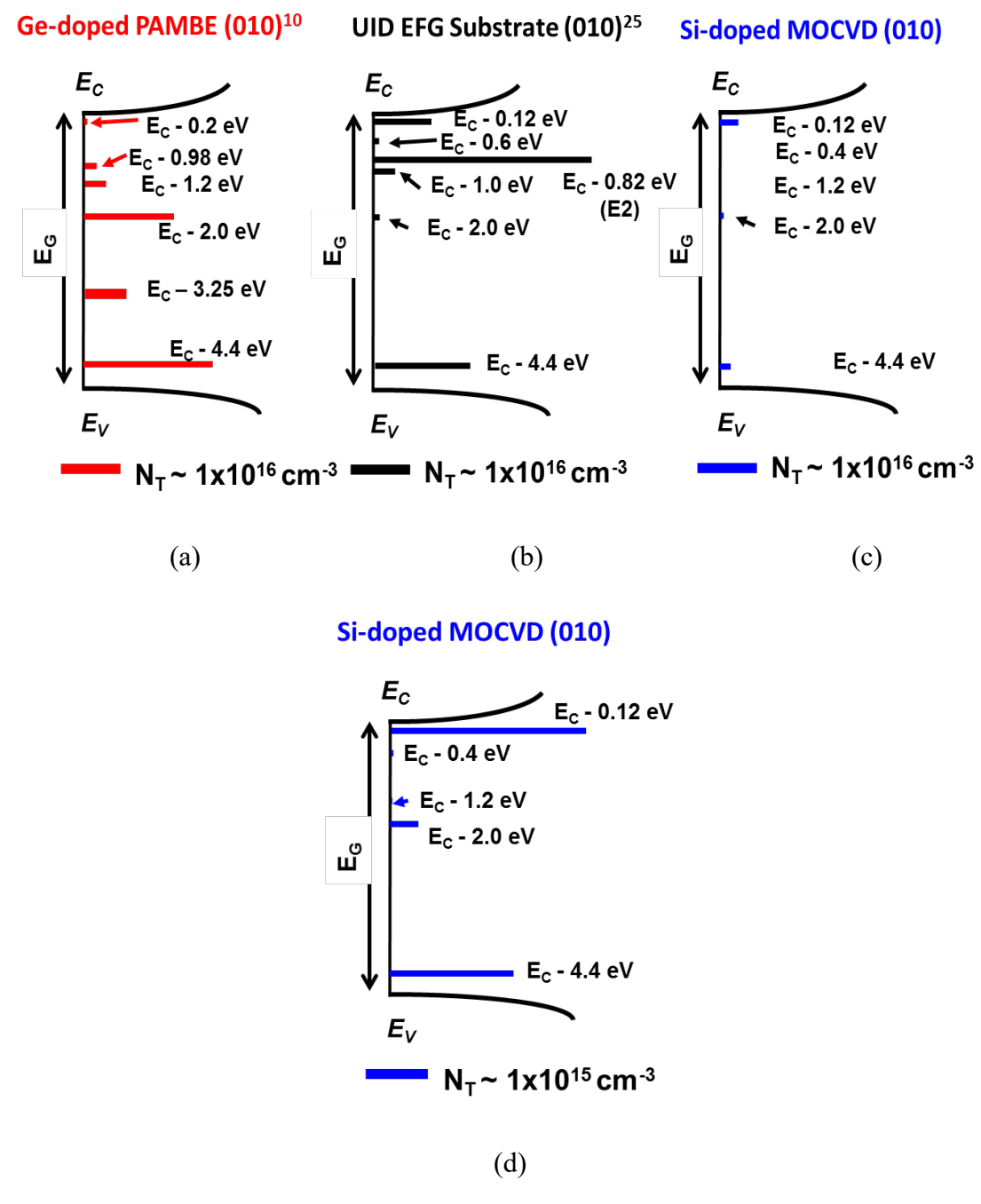


Figure 4: Summary of the energy positions and concentrations for traps detected by AS, DLTS and DLOS in β-Ga₂O₃ grown by (a) PAMBE, (b) EFG and (c) MOCVD at the same concentration scales, and (d) the MOCVD trap profile at a full scale of 10^{15} cm⁻³ (10x lower). The measurement conditions used for the respective techniques were the same in each case. Previous work has shown the E_C-0.8 eV (E2) state in the EFG material is due to residual Fe ^{27,31}, and the E_C-2.0 eV state has

been associated with gallium vacancies.³⁵ Possible correlations to physical sources for several of the other states have been summarized elsewhere. ^{10,31,33,35}

While the combination of DLTS and DLOS can provide full coverage of states within the B-Ga₂O₃ bandgap, the presence of increased ohmic contact resistance at very low temperatures for our devices (below ~ 80 K here) limits the applicability of DLTS in that range, making detection of very shallow traps (closer to E_C) difficult, especially for those states which have high carrier emission rates. This is a concern because recent transport studies on MOCVD material have implied the presence of a deep donor state at approximately E_C-0.12 eV. ²⁰ In an attempt to circumvent this issue, we resorted to admittance spectroscopy (AS) measurements since AS enables the observation of traps having relatively fast emission rates but at higher measurement temperature, thereby circumventing the contact resistance issue faced during low DLTS measurement temperature. Following prior work on admittance spectroscopy ^{39,40}, the derivative of capacitance as a function of measurement frequency reveals a peak value if a trap is present, where the peak frequency ω_p , corresponds to the trap emission rate. From this information, the trap activation energy can be extracted. Here, from figure 5 we do see the presence of a trap that has an activation energy of E_C-0.12 eV. The concentration of this trap using AS can be calculated from the change in capacitance depicted in the inset of figure 5. At lower frequencies, the measured capacitance is comprised of the depletion capacitance and is affected by the charge contribution from trap state, whereas at higher frequencies the traps cannot respond. Hence the difference between the low and high frequency capacitance provides the capacitance due to the trapping contribution alone (i.e. ΔC), through which the trap concentration was found to be 3.1×10^{15} cm⁻ ³. The concentration and activation energy of this state are in good agreement with the values extracted from transport measurements made on lightly Si-doped β-Ga₂O₃ grown by MOCVD reported earlier. ²⁰ Note that the AS data is also included in figure 4, and, as seen, is dominant in the MOCVD material. This correlation between trap spectroscopy and transport analysis reveals consistency between very different measurements, and work must now be done to explore the physical source for this defect state given its relatively high concentration compared with the other states seen by DLTS and DLOS in MOCVD-grown β-Ga₂O₃.

With the E_C -0.12 eV state clearly revealed in the Si-doped MOCVD material by AS, we decided to apply AS to β -Ga₂O₃ Schottky diodes grown using UID EFG-grown ²⁵ and Ge-doped β -Ga₂O₃ PAMBE-grown material ¹⁰, which we previously characterized by DLTS and DLOS. For the EFG material, AS revealed the same state, which is consistent with the AS work reported by Neal *et al.* ³⁹ However, there was no evidence of this state in the Ge-doped PAMBE material from these measurements. As we have previously reported for the EFG sample, SIMS revealed a background Si concentration on the order of 10^{17} cm⁻³ for the UID EFG sample, whereas SIMS showed no measurable Si concentration in Ge-doped PAMBE-grown material. Whether this state is related to the presence of Si, associated defects, or even site competition between the Ga(I) and Ga(II) sites of the β -Ga₂O₃ lattice, is under study currently.

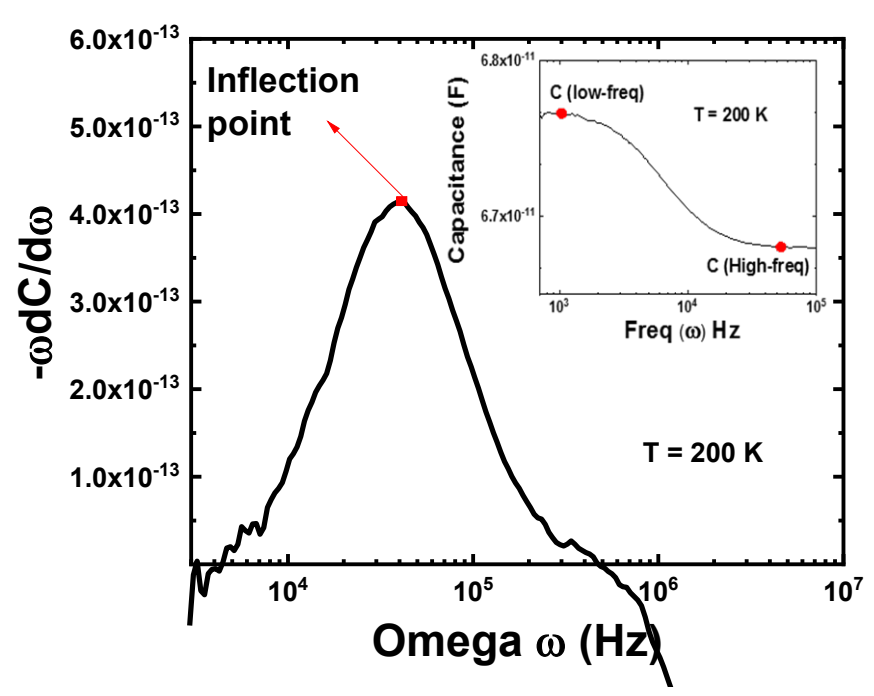


Figure 5: Inflection frequency ($\omega_p = 1/\tau$) measured at 200 K to calculate trap activation energy using $-\omega \frac{dc}{d\omega} vs \omega$ curve. Inset: Frequency dependent capacitance (C- ω) at 200 K indicating the presence of shallow defect state and required to measure $\Delta C = C(low-freq) - C(High-freq)$.

Combining the DLTS, DLOS and AS data obtained from the MOCVD-grown β -Ga₂O₃, Table 1 provides the quantitative details for all observed traps in this study, as they have not been detailed previously.

Table 1. Summary of MOCVD trap parameters obtained from AS, DLTS and DLOS measurements.

Trap Activation Energy	Trap Cross-section from AS and DLTS	D_{FC} for DLOS traps	Trap Concentration
(eV)	(cm^2)	(eV)	(cm^{-3})
E _C -0.12	7.1×10 ⁻¹⁸	-	3.1×10 ¹⁵
E_{C} -0.4	1.5×10 ⁻¹⁴	-	3×10 ¹³
E_{C} -1.2	-	0.45	1.3×10 ¹³
E_{C} -2.0	-	0.48	2.3×10 ¹⁵
E _C -4.4	-	0.06	2.1×10^{15}

In summary, a comprehensive investigation of the bandgap states in MOCVD-grown β-Ga₂O₃ was completed using a combination of DLOS, DLTS and admittance spectroscopy (AS). A large reduction in overall trap concentration was observed compared with all prior studies to date on the full bandgap spectrum of defects made on materials grown by PAMBE ¹⁰ and EFG. ²⁵ The dominant state for the MOCVD material is a relatively shallow state at E_C-0.12 eV, which was detected by AS. Its presence matches findings from previous transport studies made on MOCVD material. ²⁰ Unlike previous DLOS studies, the E_C-4.4 eV state is no longer the dominant deep state, implying that its source might be extrinsic in nature. Furthermore, DLTS revealed a previously not-reported state at E_C-0.4 eV, which exhibits ideal trapping characteristics suggestive of a simple point defect source. Moreover, proton irradiation did not affect its concentration, which implies an extrinsic source for this trap. In general, all states previously associated with an intrinsic source, including the increasingly studied E_C-2.0 eV trap, are diminished in concentration. The findings discussed here are consistent with the high electron mobilities and very low acceptor-like compensating state concentrations recently reported for MOCVD-grown β-Ga₂O₃ produced in the same reactor under identical growth conditions. These results strongly suggest that MOCVDgrown β-Ga₂O₃ has great potential to enable high performance ultra-wide bandgap electronic and optoelectronic devices.

Acknowledgement

REFERENCES:

¹ H.H. Tippins, Phys. Rev. **140**, A316 (1965).

² M. Orita, H. Ohta, M. Hirano, and H. Hosono, Appl. Phys. Lett. 77, 4166 (2000).

³ T. Onuma, S. Saito, K. Sasaki, T. Masui, T. Yamaguchi, T. Honda, and M. Higashiwaki, Jpn. J. Appl. Phys. **54**, 112601 (2015).

⁴ E. Ahmadi, O.S. Koksaldi, X. Zheng, T. Mates, Y. Oshima, U.K. Mishra, and J.S. Speck, Appl. Phys. Express **10**, 071101 (2017).

⁵ M.J. Tadjer, J.L. Lyons, N. Nepal, J.A. Freitas, A.D. Koehler, and G.M. Foster, ECS J. Solid State Sci. Technol. **8**, Q3187 (2019).

⁶ S.J. Pearton, J. Yang, P.H. Cary, F. Ren, J. Kim, M.J. Tadjer, and M.A. Mastro, Appl. Phys. Rev. **5**, 011301 (2018).

⁷ K. Sasaki, A. Kuramata, T. Masui, E.G. Víllora, K. Shimamura, and S. Yamakoshi, Appl. Phys. Express **5**, 035502 (2012).

⁸ M. Higashiwaki, K. Sasaki, A. Kuramata, T. Masui, and S. Yamakoshi, Appl Phys Lett 4 (2012).

⁹ M. Higashiwaki, K. Sasaki, T. Kamimura, M. Hoi Wong, D. Krishnamurthy, A. Kuramata, T. Masui, and S. Yamakoshi, Appl. Phys. Lett. **103**, 123511 (2013).

¹⁰ E. Farzana, E. Ahmadi, J.S. Speck, A.R. Arehart, and S.A. Ringel, J. Appl. Phys. **123**, 161410 (2018).

¹¹ N.K. Kalarickal, Z. Xia, J. McGlone, S. Krishnamoorthy, W. Moore, M. Brenner, A.R. Arehart, S.A. Ringel, and S. Rajan, Appl. Phys. Lett. **115**, 152106 (2019).

- ¹² C. Joishi, Y. Zhang, Z. Xia, W. Sun, A.R. Arehart, S. Ringel, S. Lodha, and S. Rajan, IEEE Electron Device Lett. **40**, 1241 (2019).
- ¹³ Z. Xia, H. Xue, C. Joishi, J. Mcglone, N.K. Kalarickal, S.H. Sohel, M. Brenner, A. Arehart, S. Ringel, S. Lodha, W. Lu, and S. Rajan, IEEE Electron Device Lett. **40**, 1052 (2019).
- ¹⁴ Z. Hu, K. Nomoto, W. Li, R. Jinno, T. Nakamura, D. Jena, and H. Xing, in *2019 31st Int. Symp. Power Semicond. Devices ICs ISPSD* (2019), pp. 483–486.
- ¹⁵ W. Li, Z. Hu, K. Nomoto, Z. Zhang, J.-Y. Hsu, Q.T. Thieu, K. Sasaki, A. Kuramata, D. Jena, and H.G. Xing, Appl. Phys. Lett. **113**, 202101 (2018).
- ¹⁶ K. Konishi, K. Goto, H. Murakami, Y. Kumagai, A. Kuramata, S. Yamakoshi, and M. Higashiwaki, Appl. Phys. Lett. **110**, 103506 (2017).
- ¹⁷ J. Yang, M. Xian, P. Carey, C. Fares, J. Partain, F. Ren, M. Tadjer, E. Anber, D. Foley, A. Lang, J. Hart, J. Nathaniel, M.L. Taheri, S.J. Pearton, and A. Kuramata, Appl. Phys. Lett. **114**, 232106 (2019).
- ¹⁸ Y. Zhang, Z. Xia, C. Joishi, and S. Rajan, in *2018 76th Device Res. Conf. DRC* (2018), pp. 1–2.
- ¹⁹ K.D. Chabak, J.P. McCandless, N.A. Moser, A.J. Green, K. Mahalingam, A. Crespo, N. Hendricks, B.M. Howe, S.E. Tetlak, K. Leedy, R.C. Fitch, D. Wakimoto, K. Sasaki, A. Kuramata, and G.H. Jessen, IEEE Electron Device Lett. **39**, 67 (2018).
- ²⁰ Z. Feng, A.F.M. Anhar Uddin Bhuiyan, M.R. Karim, and H. Zhao, Appl. Phys. Lett. **114**, 250601 (2019).
- ²¹ Y. Zhang, F. Alema, A. Mauze, O.S. Koksaldi, R. Miller, A. Osinsky, and J.S. Speck, APL Mater. 7, 022506 (2019).
- E. Ahmadi, O.S. Koksaldi, S.W. Kaun, Y. Oshima, D.B. Short, U.K. Mishra, and J.S. Speck, Appl. Phys. Express 10, 041102 (2017).
 N. Ma, N. Tanen, A. Verma, Z. Guo, T. Luo, H. (Grace) Xing, and D. Jena, Appl. Phys. Lett.
- ²³ N. Ma, N. Tanen, A. Verma, Z. Guo, T. Luo, H. (Grace) Xing, and D. Jena, Appl. Phys. Lett. **109**, 212101 (2016).
- ²⁴ A. Fiedler, R. Schewski, M. Baldini, Z. Galazka, G. Wagner, M. Albrecht, and K. Irmscher, J. Appl. Phys. **122**, 165701 (2017).
- ²⁵ Z. Zhang, E. Farzana, A.R. Arehart, and S.A. Ringel, Appl. Phys. Lett. **108**, 052105 (2016).
- ²⁶ J.B. Varley, J.R. Weber, A. Janotti, and C.G. Van de Walle, Appl. Phys. Lett. **97**, 142106 (2010).
- ²⁷ M.E. Ingebrigtsen, J.B. Varley, A.Yu. Kuznetsov, B.G. Svensson, G. Alfieri, A. Mihaila, U. Badstübner, and L. Vines, Appl. Phys. Lett. **112**, 042104 (2018).
- ²⁸ P. Blood and J.W. Orton, in (1992).
- ²⁹ D.V. Lang, J. Appl. Phys. **45**, 3023 (1974).
- ³⁰ R. Pässler, J. Appl. Phys. **96**, 715 (2004).
- ³¹ J.F. Mcglone, Z. Xia, Y. Zhang, C. Joishi, S. Lodha, S. Rajan, S.A. Ringel, and A.R. Arehart, IEEE Electron Device Lett. **39**, 1042 (2018).
- ³² A. Chantre, G. Vincent, and D. Bois, Phys. Rev. B **23**, 5335 (1981).
- ³³ E. Farzana, M.F. Chaiken, T.E. Blue, A.R. Arehart, and S.A. Ringel, APL Mater. 7, 022502 (2019).
- ³⁴ J.B. Varley, H. Peelaers, A. Janotti, and C.G. Van de Walle, J. Phys. Condens. Matter **23**, 334212 (2011).
- ³⁵ J.M. Johnson, Z. Chen, J.B. Varley, C.M. Jackson, E. Farzana, Z. Zhang, A.R. Arehart, H.-L. Huang, A. Genc, S.A. Ringel, C.G. Van de Walle, D.A. Muller, and J. Hwang, ArXiv190700563 Cond-Mat (2019).

- ³⁶ A. Armstrong, J. Caudill, A. Corrion, C. Poblenz, U.K. Mishra, J.S. Speck, and S.A. Ringel, J. Appl. Phys. 103, 063722 (2008).
- ³⁷ J.B. Varley, A. Janotti, C. Franchini, and C.G. Van de Walle, Phys. Rev. B **85**, 081109 (2012). ³⁸ A.M. Armstrong, M.H. Crawford, A. Jayawardena, A. Ahyi, and S. Dhar, J. Appl. Phys. **119**, 103102 (2016).
- ³⁹ A.T. Neal, S. Mou, R. Lopez, J.V. Li, D.B. Thomson, K.D. Chabak, and G.H. Jessen, Sci. Rep. **7**, (2017).
- 40 S. Khelifi, K. Decock, J. Lauwaert, H. Vrielinck, D. Spoltore, F. Piersimoni, J. Manca, A. Belghachi, and M. Burgelman, J. Appl. Phys. 110, 094509 (2011).